# Interplay between charge density wave and antiferromagnetic order in $GdNiC_2$

N. Hanasaki*
*Department of Physics, Osaka University, Toyonaka 560-0043, Japan*

S. Shimomura
*Department of Physics, Kyoto Sangyo University, Kyoto 603-8555, Japan*

K. Mikami and Y. Nogami
*Department of Physics, Okayama University, Okayama 700-8530, Japan*

H. Nakao
*Condensed Matter Research Center and Photon Factory, Institute for Material Structural Science, High Energy Accelerator Research Organization, Tsukuba 305-0801, Japan*

H. Onodera
*Institute for Materials Research, Tohoku University, Sendai 980-8577, Japan*

(Received 31 July 2016; revised manuscript received 31 December 2016; published 2 February 2017)

The correlation between the charge density wave (CDW) and $f$ local moments is observed in $GdNiC_2$ by means of x-ray diffraction in a magnetic field. Various kinds of electronic states exist in the magnetic field. The intensity of the CDW peak changes in the successive transitions and the commensurate-incommensurate transition of the CDW takes place as well. The successive transitions are explained in terms of a cooperative effect of the Peierls instability and the spin Friedel oscillation, in which the antiferromagnetic order of the $f$ local moments is coupled to the spin density wave coexisting with the CDW of the conduction electron.

DOI: 10.1103/PhysRevB.95.085103

## I. INTRODUCTION

The interplay between the electron conduction and the local moments is a central topic in condensed matter physics. This interaction gives rise to interesting phenomena such as giant magnetoresistance and heavy fermions [1–3]. The interaction with local moments is also attractive in a low-dimensional electron system, in which the Peierls instability gives rise to the charge-density-wave (CDW) state and the spin-density-wave (SDW) state [4]. If the local moments exist on this conducting path, the antiferromagnetic coupling ($J_{cf}$) with the conduction electron induces the spin Friedel oscillation, in which the spin density oscillates with the wave number of $2k_F$ [5,6]. Since the Peierls instability also has a singularity in the wave vector of $2k_F$, one can expect a cooperative effect of the density waves and the magnetic order of the $f$ local moments [7,8]. In several rare-earth compounds, coexistence of the density wave state and the antiferromagnetic order of the $f$ moment has been reported [9]. Unfortunately, the cooperative phenomena by which the creation of an $f$-moment order induces a drastic change in the CDW order parameter have not been adequately clarified. Recently, it was reported that the CDW state is correlated with the magnetic order of the $f$ moments. In $SmNiC_2$, the CDW is destroyed in the ferromagnetic (FM) transition [10]. This phase competition enables us to critically control the electronic state by applying a magnetic field [11]. In $GdNiC_2$, the intensity of the CDW peak changes in the antiferromagnetic (AFM) transition of the $f$ local moments [12]. In contrast to the FM state, the CDW coexists with the AFM state. It is found that the wave vector of this CDW agrees with that of the AFM order of the $f$ moments in $TbNiC_2$ [12,13]. However, the microscopic mechanism underlying the correlation between the CDW and the magnetic orders remains unclear.

The magnetic-field effect gives a clue toward the clarification of the correlation mechanism, since the magnetic field can control the magnetic state; hence this influence upon the CDW can be examined. The $GdNiC_2$ is a suitable system for this research, since the Gd $f$ local moment, which has almost no magnetic anisotropy due to the orbital component, is very susceptible to a magnetic field. Indeed, the successive transitions take place in the magnetic field [14]. In this paper, we report our direct observation of a correlation between the CDW state and the $f$ local moment by means of x-ray diffraction in the magnetic field and propose a correlation mechanism for the CDW and the $f$-moment orders. This correlation can be explained in terms of a cooperative effect of the Peierls instability and the spin Friedel oscillation, taking into account the role of the SDW in creating the $f$-moment order.

As shown in the inset of Fig. 1(b), the Gd, the Ni, and the dimer of C stack along the $a$ axis, and form triangular lattices in the $bc$ plane [15]. This crystal system is $Amm2$ and does not have space inversion symmetry. According to the band calculation [16], a part of the Fermi surface (FS) is a warping sheet parallel to the $b^*c^*$ plane. Since the density of states (DOS) near the Fermi level ($E_F$) comes from only the $3d$ orbital of the Ni and the $4d$ orbital of the rare earth, these $d$ electrons contribute to the electron conduction, while the $f$ electron of the rare earth is localized.

*hanasaki@phys.sci.osaka-u.ac.jp

 ©2017 American Physical Society

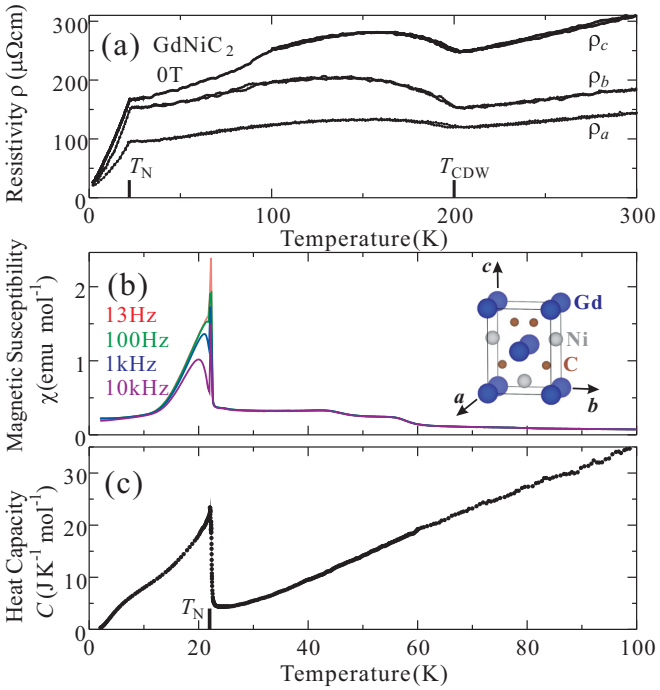


FIG. 1. Temperature dependence of the physical properties in 0 T in $GdNiC_2$. (a) Resistivity $\rho$ measured under the current applied along the $a$, $b$, and $c$ axes. (b) Magnetic susceptibility $\chi$ measured in an ac magnetic field (3 G) applied along the $c$ axis. Inset: Crystal structure of $GdNiC_2$. (c) Heat capacity $C$. The bottom bars in $T_N$ and $T_{CDW}$ indicate the AFM and CDW transition temperatures, respectively.

## II. EXPERIMENT

The single crystal of $GdNiC_2$ was grown by using an arc furnace. We measured the resistivity, the magnetization, and the heat capacity using Quantum Design PPMS. The molar unit of the magnetic susceptibility is one formula unit of $GdNiC_2$. The x-ray diffraction was measured at the Photon Factory BL-3A.

## III. RESULTS AND DISCUSSION

Figure 1(a) displays the temperature dependence of the resistivity $\rho$. The resistivity increases below 200 K [12]. Below this $T_{CDW}$, the satellite of the x-ray diffraction due to the CDW is observed [10]. The wave number of this satellite is (0.5, ≈0.5, 0), which is consistent with the band calculation [16]. The resistivity remains at a low value below $T_{CDW}$, suggesting the imperfect nesting of the CDW. The magnetic susceptibility $\chi$ [Fig.1(b)] also shows an anomaly at the AFM transition temperature $T_N = 22$ K [17]. A clear peak of the heat capacity $C$ [Fig.1(c)] also provides thermodynamical evidence of the AFM transition.

We investigated the magnetic-field effect on this AFM state. At 2 K, as indicated by the arrow in Fig. 2(a), the spin flop occurs near 1.2 T [14,17]. The metamagnetic transition is also observed near $B_{MM} \approx 6$ T. We summarize the phase diagram in Fig. 3(a) on the basis of the magnetization anomalies. The boundary between the antiferromagnetic phase 1 (AFM1) and the AFM2 corresponds to the spin-flop field. We refer to the metamagnetic state above $B_{MM}$ as the MM state.

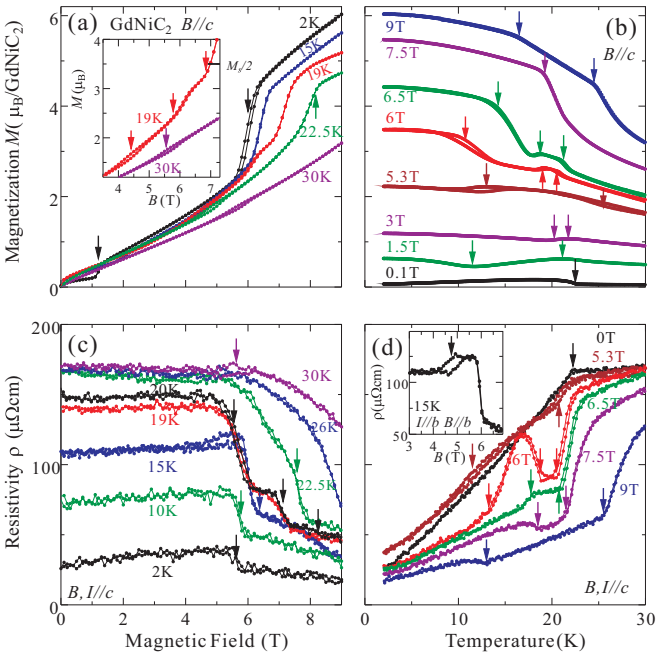


FIG. 2. (a, c) Magnetic-field dependence of the magnetization $M$ (a) and the resistivity $\rho$ (c) in $GdNiC_2$. The arrows indicate the anomalies related to the phase transitions. The right horizontal bar in the inset indicates the half of the full moment $M_s$ per $GdNiC_2$. (b, d) Temperature dependence of $M$ (b) and $\rho$ (d). The magnetic field is applied along the $c$ axis. The resistivity shown in the main panels and the inset was measured under the current applied along the $c$ axis and the $b$ axis, respectively.

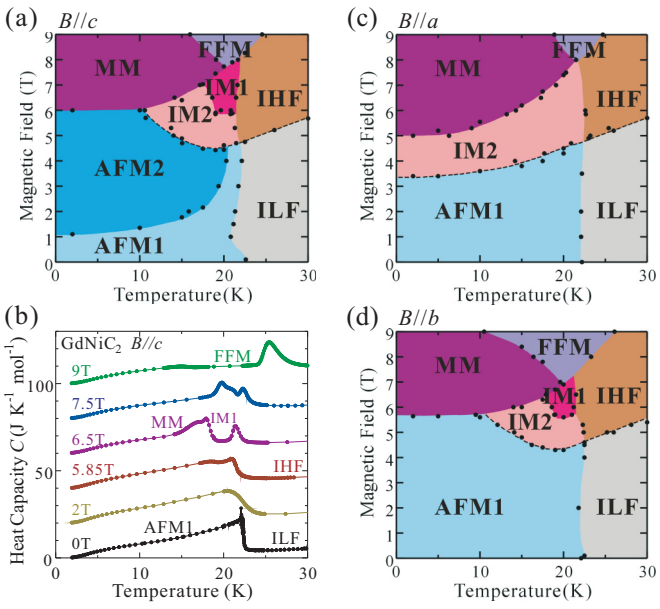


FIG. 3. (a) Magnetic-field-temperature phase diagram in $GdNiC_2$ in the magnetic field applied along the $c$ axis. Here, AFM, MM, IM, FFM, and IL(H)F denote the antiferromagnetic, metamagnetic, intermediate, forced-ferromagnetic, and intermediate-temperature–low(high)-magnetic-field phases, respectively. (b) Heat capacity $C$ measured in the magnetic field applied along the $c$ axis. The data were offset by 20 J $K^{-1}$ $mol^{-1}$ for visibility. (c, d) Phase diagram in the magnetic field applied along the $a$ axis (c) and the $b$ axis (d).

Next, we show the intermediate states characteristic of $GdNiC_2$. The magnetization also has an anomaly with the hysteresis near 4.5 T at 19 K in the inset of Fig. 2(a), and at ≈11 K near 6 T in Fig. 2(b). Thus, the intermediate state 2 (IM2) exists above ≈4.5 T and ≈11 K. The ramp is seen near $B = 6$–7 T at 19 K in the inset of Fig. 2(a). The hump is observed for $T = 18$ K to 22 K near 6.5 T in Fig. 2(b). The electronic state related to this hump, whose magnetization value is close to half of the saturation moment $M_s$ (≈7 $\mu_B$ [17]), is termed the intermediate1 (IM1) phase. The origin of these IM phases is discussed later.

Above $T_N = 22$ K, the electronic state seems paramagnetic. A close look reveals that the anomaly with the hysteresis is seen only near $B = 5 \sim 6$ T at 30 K in the inset of Fig. 2(a). This anomaly separates this paramagnetic state into the intermediate-temperature–low-field (ILF) state and the intermediate-temperature–high-field (IHF) state.

We also examined the phase diagram of Fig. 3(a), by measuring the resistivity $\rho$. As shown in Fig. 2(c), at 2 K and 10 K, the resistivity drops near 5.7 T, which corresponds to the critical field ($B_{MM}$) between the AFM2 and the MM phases. At 20 K, after the resistivity decreases rapidly near $B = 5 \sim 6$ T, it reaches a plateau, and then drops again near 7 T. This magnetic-field range ($B = 6 \sim 7$ T) of the resistivity plateau corresponds to that of the magnetization ramp in the IM1 phase [the inset of Fig. 2(a)]. Figure 2(d) displays the temperature dependence of the resistivity. At 6 T, the resistivity exhibits anomalous behavior; as the temperature is lowered, the resistivity drops at ≈21 K, rises at ≈18.5 K, and then decreases again below ≈16 K. This low-resistivity region between ≈18.5 K and 21 K corresponds to the IM1 phase, while the high-resistivity region between ≈13 K and 18.5 K is related to the IM2 state. The clear hysteresis suggests the first-order transitions. At 9 T, the kink structure is seen at 13 K and 25.5 K. Since the region between these kinks becomes stable in the higher fields, this state is considered the forced-ferromagnetic (FFM) phase. There is a slight difference in the anomaly between the resistivity and the magnetization measurements. For example, at 6.5 T, the magnetization dip due to the IM1 phase is seen around 17 K in Fig. 2(b), while the resistivity peak due to the IM1 phase is not observed in Fig. 2(d). At 7.5 T, the resistivity anomalies due to the FFM phase are seen at 19 K and 21 K in Fig. 2(d), while the magnetization anomaly is seen only at 19 K in Fig. 2(b). It is because there is hysteresis in the phase transition, and then the resistivity measurement can detect the low-resistive state more easily than the magnetization measurement on the phase boundary. Figure 3(b) shows the heat capacity $C$. In the zero field, the heat capacity shows a clear peak at $T_N = 22$ K. At 6.5 T, the peaks appear not only at 21.3 K, indicating the transition between the IHF and IM1 phases, but also at 18 K, suggesting the transition between the IM1 and MM phases. At 9 T, the anomalies near 15 K and 25.5 K indicate the transition related to the FFM phase.

Figures 4(a) and 4(d) show the CDW satellite profiles and their intensities $I_q$ observed near (0.5, 3.5, 0) at 5 K, respectively. In the AFM1 and the AFM2 states, the intensity $I_q$ gradually decreases with the magnetic field. Then, the $I_q$ falls to zero near $B_{MM} \approx 6$ T, suggesting the total disappearance of the CDW. In $SmNiC_2$, we also observed the FM-induced

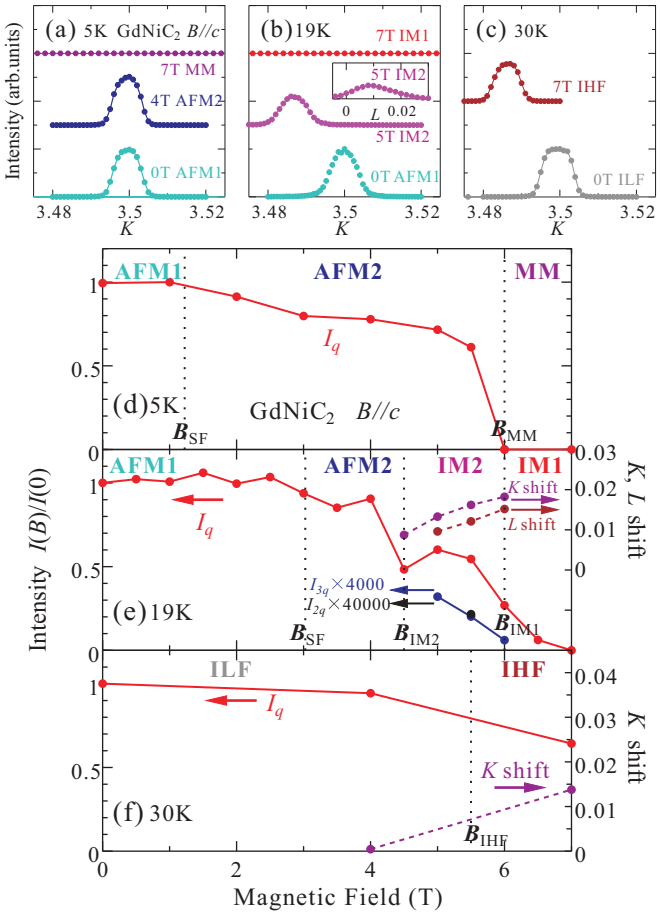


FIG. 4. (a)–(c) Satellite in the x-ray diffraction observed in (0.5, ≈3.5, ≈0) in the magnetic field in $GdNiC_2$. The $K$ scans at 5 K, 19 K, and 30 K are displayed in panels (a), (b), and (c), respectively. Inset: $L$ scan at 5 T at 19 K. (d)∼(f) Magnetic-field dependence of the satellite intensity normalized by the zero-field one (red lines), the $K$ shift (violet dashed line), and the $L$ shift (brown dashed line) at 5 K (d), 19 K (e), and 30 K (f). The second and third harmonic components are shown by the black and blue points in panel (e), respectively. The magnetic field was applied along the $c$ axis.

disappearance of the CDW [10,11]. After the spin flop of the Gd moments takes place near 1.2 T applied along the $c$ axis, the directions of the Gd moments become nearly perpendicular to the $c$ axis in the AFM2 phase. Above $B_{MM} \approx 6$ T, all the Gd moments are tilted toward the magnetic fields, and the magnetic state approaches the forced ferromagnetic one. This spin polarization changes the band structure and makes the FS nesting impossible [10,11]. The FM effect on the CDW is also discussed in the IM1 state later.

Figures 4(b) and 4(e) display the peak profiles, their intensities, and their wave numbers at 19 K. At $B_{IM2} \approx 4.5$ T, the intensity $I_q$ becomes nearly half of the zero-field one. The wave numbers $K$ and $L$ become incommensurate, as shown by the violet and brown dashed lines. After this commensurate-incommensurate (C-IC) transition, the second and third harmonic components ($I_{2q}$ and $I_{3q}$) appear as well. Then, above $B_{IM1} \approx 6$ T, the intensity approaches zero, indicating the disappearance of the CDW. In Figs. 4(c) and 4(f), we display the satellite profiles, their intensities, and their

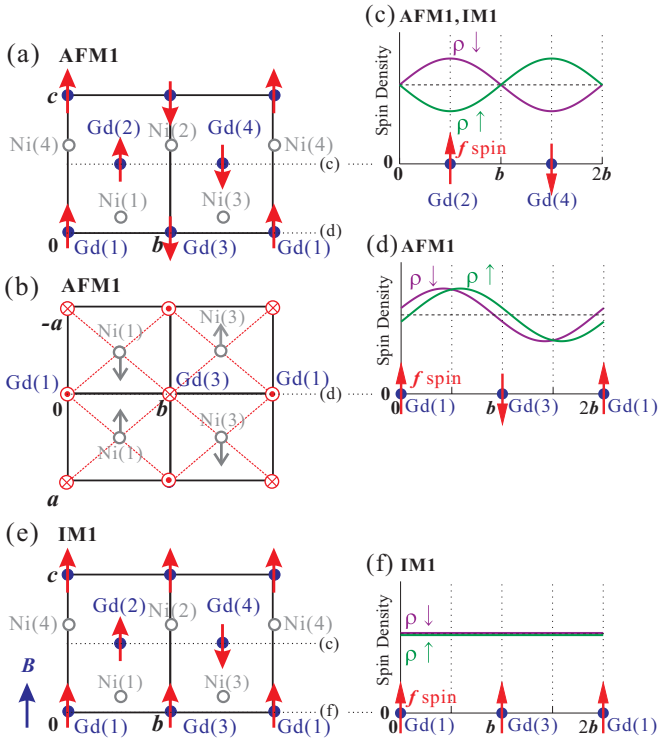


FIG. 5. (a)–(d) AFM1 phase. (a, b) Schematic of the Gd $f$ moments (red arrows) and the Ni displacement (gray arrows). (c, d) Up-spin density $\rho_\uparrow$ (green) and down-spin density $\rho_\downarrow$ (violet) of the conduction electron. Here, the positions in panels (c) and (d) correspond to those on the black dotted line labeled with (c) and (d) in panels (a) and (b). (c, e, f) IM1 phase. Here, the positions in panels (c) and (f) correspond to those on the black dotted line labeled with (c) and (f) in panel (e), respectively.

wave numbers at 30 K. In the boundary ($B_{\rm IHF}$) between the ILF and IHF phases, the C-IC transition occurs. In the IHF state, the $K$ components are incommensurate. The $I_q$ decreases and remains a finite value.

Let us discuss the spin structure in the AFM1 state. In the isostructural compound $TbNiC_2$, the neutron diffraction shows the AF order of the $f$ moments, whose period is $2a$ and $2b$ along the $a$ and $b$ axes, respectively [13,18]. This $f$ spin structure is created by the RKKY interaction determined by the shape of the Fermi surface. The band calculation suggests that the band structure in $TbNiC_2$ is similar to that in $GdNiC_2$ [16]. Thus, the Gd $f$ spin is anticipated to have a spin structure similar to that of $TbNiC_2$. Four kinds of Gd spins are oriented in the direction close to the $c$ axis in the AFM1 state, as suggested by the Mössbauer experiment [17]. In Figs. 5(a) and 5(b), we present possible models of the Gd $f$ spin configuration. Here, for the simplicity, the $f$ moments (red arrows) are drawn so that the $f$ moments are parallel or antiparallel to the $c$ axis.

Taking into account the CDW structure suggested by Wölfel *et al.* [19] and the $J_{cf}$ interaction with the $f$ moments, we propose up- and down-spin densities ($\rho_\uparrow$ and $\rho_\downarrow$) of the conduction electron in the AFM1 phase, as shown in Figs. 5(c) and 5(d). The charge density ($\rho_{\rm charge} = \rho_\uparrow + \rho_\downarrow$) is the sum of the up-spin density $\rho_\uparrow$ and the down-spin density $\rho_\downarrow$. As shown in Fig. 5(d), the charge density oscillates in the $ab$ plane of the Gd(1) and Gd(3) sites, whose plane is close to the Ni(1) and Ni(3) atoms [Fig. 5(a)]. Since the charge densities reach maxima (minima) near the middle of the Ni(1) [Ni(3)] atoms, the Ni(1) and Ni(3) atoms are displaced [Fig. 5(b)], and the CDW is formed in these Ni chains along the $a$ axis. As shown in Fig. 5(c), the charge density remains constant in the $ab$ plane of the Gd(2) and Gd(4) atoms, whose plane is close to the Ni(2) and Ni(4) atoms [Fig. 5(a)]. The Ni(2) and Ni(4) chains cannot contribute to the CDW, and these Ni atoms are not displaced. Wölfel *et al.* suggested that frustration existed between the CDWs in each Ni chain [19].

Through the $J_{cf}$ interaction, the AFM order of the $f$ moments is antiferromagnetically coupled to the oscillation of the spin density ($\rho_{\rm spin} = \rho_\uparrow - \rho_\downarrow$) of the conduction electron [Figs. 5(c) and 5(d)], which is given by the difference between the up-spin density $\rho_\uparrow$ and the down-spin density $\rho_\downarrow$. This spin density oscillation (wave) is generated by the different phase shift of the up- and down-spin density composing the CDW, and the wave vector of this SDW agrees with that of the CDW [20]. From a different point of view, the $J_{cf}$ interaction induces a local spin Friedel oscillation with a wave number of $2k_F$ of the conduction electron around the $f$ local moment, and the Peierls instability is expected to amplify this spin density oscillation to form the long-range SDW state [8]. As a result, the SDW causes the AFM order of the $f$ moments through the $J_{cf}$ interaction.

In the IM1 phase, as discussed in Fig. 4(e), at 19 K the CDW disappears above $B_{\rm IM1} \approx 6$ T. As displayed in Fig. 2(c), the resistivity decreases by $\approx$70 $\mu\Omega$ cm at $B = 5 \sim 6$ T ($\approx B_{\rm IM1}$). The resistivity is, roughly speaking, proportional to the inverse of the DOS($E_F$). The resistivity in the IM1 phase is higher by $\approx$30 $\mu\Omega$ cm than that in the FFM phase, in which neither the CDW nor the SDW exist above $B_{\rm FFM} \approx 8$ T. This difference in resistivity between the IM1 and the FFM phases indicates the existence of a gap in the IM1 phase. One possible origin of this gap might be the remnant SDW. As shown in the inset of Fig. 2(a), the magnetization value in the IM1 phase is close to half of the full moment $M_s$. This suggests that three-quarters of the Gd $f$ moments are parallel to the magnetic-field direction (the $c$ axis), while a quarter of the Gd moments are antiparallel to it. Figures 5(e) and 5(f) illustrate a possible structure of the Gd $f$ moments and the spin densities in the IM1 phase. The $f$ moment in Gd(1) is parallel to that in Gd(3). This FM configuration suppresses both the CDW and the SDW in the Gd(1)-Gd(3) plane through the $J_{cf}$ interaction. In the Gd(2)-Gd(4) plane, as shown in Figs. 5(c) and 5(e), the AFM order of the $f$ moments and the SDW state remain.

In the IM2 phase, the incommensurate CDW exists, and the $K$ and $L$ components have incommensurate values. When the current is applied along the $b$ axis, as shown in the inset of Fig. 2(d), the resistivity in the IM2 phase is higher than that in the AFM1 and the AFM2 states. This indicates that the nesting vector changes so that the nesting conditions improve. The theoretical studies suggest that the commensurate-incommensurate CDW transition can take place in the magnetic fields through the Zeeman effect [21,22]. The IHF phase is also stable in the magnetic field, and the $K$ component has an incommensurate value as well. The phase boundary between the IM2 and AFM states is smoothly linked to that between the ILF and IHF states, as

indicated by the dashed curve in Fig. 3(a). The mechanism of the incommensurate $K$ value in the IHF phase may be similar to that in the IM2 phase.

Figures 3(c) and 3(d) display the phase diagram in the magnetic field parallel to the $a$ axis and the $b$ axis on the basis of the magnetization anomalies, respectively. The spin flop is observed only when the magnetic field is applied along the $c$ axis, which is the magnetic easy axis. The IM1 phase does not exist in the magnetic field parallel to the $a$ axis, as shown in Fig. 3(c). Since the $a$ axis is the magnetic hard axis, in the magnetic field parallel to the $a$ axis, it is impossible to form the spin configuration such as the IM1 phase illustrated in Fig. 5(e), in which one spin of four spins is oriented towards the opposite direction with respect to the magnetic field. The phase boundary between the IM2 and AFM states is smoothly linked to that between the ILF and IHF states, as indicated by the dashed curve in Figs. 3(c) and 3(d) as well.

## IV. CONCLUSIONS

We observed a change of the CDW order parameter caused by the magnetic transition of the $f$ moments. The SDW is given by the phase shift of the spin density in the CDW and is correlated with the $f$-moment order. In the higher fields, the intensity of the CDW peak changes in the successive transitions, and the commensurate-incommensurate CDW transition takes place as well. The successive transitions are explained in terms of the above correlation mechanism.

## ACKNOWLEDGMENTS

The authors thank K. Machida, H. Kawamura, Y. Yamasaki, and Y. Murakami for valuable discussion and K. Yokota and T. Tateishi for experimental support in x-ray diffraction in a high magnetic field. This work was partly supported by JSPS KAKENHI Grants No. JP16K13838, No. JP24540374, and No. JP22540373 and by the Priority Area "Novel States of Matter Induced by Frustration" (JSPS KAKENHI Grant No. JP19052003). This work was performed under the approval of the Photon Factory Program Advisory Committee (Proposals No. 2009G025 and No. 2011G101). This work was partly carried out at the Center for Spintronics Research Network (CSRN), Graduate School of Engineering Science, Osaka University, Machikaneyama 1-3, Toyonaka, Osaka 560-8531, Japan.

[1] M. N. Baibich, J. M. Broto, A. Fert, F. Nguyen Van Dau, F. Petroff, P. Etienne, G. Creuzet, A. Friederich, and J. Chazelas, Phys. Rev. Lett. **61**, 2472 (1988).
[2] K. L. Kobayashi, T. Kimura, H. Sawada, K. Terakura, and Y. Tokura, Nature (London) **395**, 6703 (1998).
[3] G. R. Sewart, Rev. Mod. Phys. **56**, 755 (1984).
[4] G. Grüner, *Density Waves in Solids* (Addision-Wesley, Reading, MA, 1994).
[5] M. A. Ruderman and C. Kittel, Phys. Rev. **96**, 99 (1954); T. Kasuya, Prog. Theor. Phys. **16**, 45 (1956); K. Yoshida, Phys. Rev. **106**, 893 (1957).
[6] S. Minami and H. Kawamura, J. Phys. Soc. Jpn. **84**, 044702 (2015).
[7] Y. Feng, J. Wang, D. M. Silevitch, J. W. Kim, J.-Q. Yan, R. K. Schulze, N. Woo, A. Palmer, Y. Ren, J.van Wezel, P. B. Littlewood, and T. F. Rosenbaum, Proc. Natl. Acad. Sci. USA **110**, 3287 (2013).
[8] D. S. Inosov, D. V. Evtushinsky, A. Koitzsch, V. B. Zabolotnyy, S. V. Borisenko, A. A. Kordyuk, M. Frontzek, M. Loewenhaupt, W. Löser, I. Mazilu, H. Bitterlich, G. Behr, J.-U. Hoffmann, R. Follath, and B. Büchner, Phys. Rev. Lett. **102**, 046401 (2009).
[9] F. Galli, S. Ramakrishnan, T. Taniguchi, G. J. Nieuwenhuys, J. A. Mydosh, S. Geupel, J. Lüdecke, and S.van Smaalen, Phys. Rev. Lett. **85**, 158 (2000).
[10] S. Shimomura, C. Hayashi, G. Asaka, N. Wakabayashi, M. Mizumaki, and H. Onodera, Phys. Rev. Lett. **102**, 076404 (2009).
[11] N. Hanasaki, Y. Nogami, M. Kakinuma, S. Shimomura, M. Kosaka, and H. Onodera, Phys. Rev. B **85**, 092402 (2012).
[12] S. Shimomura, C. Hayashi, N. Hanasaki, K. Ohnuma, Y. Kobayashi, H. Nakao, M. Mizumaki, and H. Onodera, Phys. Rev. B **93**, 165108 (2016).
[13] H. Onodera, N. Uchida, M. Ohashi, H. Yamaguchi, and N. Sato, J. Magn. Magn. Mater. **137**, 35 (1994).
[14] N. Hanasaki, K. Mikami, S. Torigoe, Y. Nogami, S. Shimomura, M. Kosaka, and H. Onodera, J. Phys.: Conf. Ser. **320**, 012072 (2011).
[15] W. Jeitscko and M. H. Gerss, J. Less-Common Met. **116**, 147 (1986).
[16] J. Laverock, T. D. Haynes, C. Utfeld, and S. B. Dugdale, Phys. Rev. B **80**, 125111 (2009).
[17] S. Matsuo, H. Onodera, M. Kosaka, H. Kobayashi, M. Ohashi, H. Yamaguchi, and T. Yamaguchi, J. Magn. Magn. Mater. **161**, 255 (1996).
[18] J. K. Yakinthos, P. A. Kotsanidis, W. Schäfer, and G. Will, J. Magn. Magn. Mater. **81**, 163 (1989).
[19] A. Wölfel, L. Li, S. Shimomura, H. Onodera, and S. van Smaalen, Phys. Rev. B **82**, 054120 (2010).
[20] N. Kobayashi and M. Ogata, J. Phys. Soc. Jpn. **66**, 3356 (1997).
[21] M. Fujita, K. Machida, and H. Nakanishi, J. Phys. Soc. Jpn. **54**, 3820 (1985).
[22] D. Zanchi, A. Bjelis, and G. Montambaux, Phys. Rev. B **53**, 1240 (1996).